The streaming potential of liquid carbon dioxide in Berea sandstone

Jeffrey R. Moore
University of California, Berkeley
S D. Glaser
H F. Morrison
G M. Hoversten

The streaming potential of liquid carbon dioxide in Berea sandstone

Abstract

We report here, for the first time, evolution of the streaming potential coupling coefficient as liquid carbon dioxide infiltrates Berea sandstone. Using 125 Omega-m tap water, the coupling coefficient determined before and after each CO2 flood of five samples averaged approximately -30 mV/0.1 MPa. After liquid CO2 passed through the specimens displacing all mobile pore water, trapped water remained and the coupling coefficient was approximately -3 mV/0.1 MPa. A bound water limit of the coupling coefficient for liquid CO2 flow was found using an air-dried sample to be -0.02 mV/0.1 MPa. For initially water-saturated samples, bulk resistivity varied during CO2 invasion from 330 Ohm-m, to 150 Ohm-m during CO2/water mixing, to a final value of 380 Ohm-m. Results suggest that trapped and bound water control electrical conduction and the electrokinetic response. Applications include monitoring CO2 injectate in subsurface reservoirs using the self potential method.

The Streaming Potential of Liquid Carbon Dioxide in Berea Sandstone

Jeffrey R. Moore[1], Steven D. Glaser[1], H. Frank Morrison[1], and G. Michael Hoversten[2]*
[1]University of California, Berkeley, Civil and Environmental Engineering
[2]Lawrence Berkeley National Laboratory, Earth Science Division
*email: moore@decf.berkeley.edu

Abstract

We report here, for the first time, evolution of the streaming potential coupling coefficient as liquid carbon dioxide infiltrates Berea sandstone. Using 125 Ω-m tap water, the coupling coefficient determined before and after each CO_2 flood of five samples averaged approximately −30 mV / 0.1MPa. After liquid CO_2 passed through the specimens displacing all mobile pore water, trapped water remained and the coupling coefficient was approximately −3 mV / 0.1MPa. A bound water limit of the coupling coefficient for liquid CO_2 flow was found using an air-dried sample to be −0.02 mV / 0.1MPa. For initially water-saturated samples, bulk resistivity varied during CO_2 invasion from 330 Ω-m, to 150 Ω-m during CO_2 / water mixing, to a final value of 380 Ω-m. Results suggest that trapped and bound water control electrical conduction and the electrokinetic response. Applications include monitoring CO_2 injectate in subsurface reservoirs using the self potential method.

1. Introduction

In response to global climate change caused by the buildup of greenhouse gasses, several schemes have been proposed to inject liquefied atmospheric CO_2 into the earth for sequestration. For these schemes to be approached rationally, the location of the injectate must be mapped through time. Self potential, in this case streaming potential (SP), is a widely recognized method for identifying flow paths through rock and soil matrices (Corwin and Hoover, 1979; Fagerlund and Heinson, 2002).

Modeling the SP response to CO_2 injection requires knowledge of the coupling parameter between fluid-pressure gradient and electrical current density (Sill, 1983). Typically this value is determined in the laboratory for specific scenarios including varying pore fluid properties (e.g. Alkafeef et al., 1999). For this experiment we analyzed the SP response resulting from displacement of in situ pore water by an advancing liquid CO_2 front, mimicking CO_2 injection into subsurface aquifers. We used intact specimens of Berea sandstone as a representative reservoir rock.

Throughout this work we refer to various states of water saturation. We denote *trapped water* to be water which remains in an initially saturated sample after all *mobile water* has drained. Specifically, as CO_2 invades the specimen *mobile water* drains until eventually no more water leaves the sample. At this point only *trapped water* remains and may be contained in the microporosity of kaolinite aggregates which are abundant in Berea sandstone. Distinct from this is *bound water*, which refers to those layers of water molecularly adsorbed onto mineral grain surfaces that can only be removed by heating and high vacuum.

2. Electrokinetic Phenomena

The laws controlling linear transport in porous media in the presence of electrokinetic coupling are (Pride, 1994):

$$\boldsymbol{q} = -L_{11}\nabla p - L_{12}\nabla\varphi \qquad (1)$$

$$\boldsymbol{j} = -L_{21}\nabla p - L_{22}\nabla\varphi \qquad (2)$$

where $\boldsymbol{q}$ is the volumetric fluid flow density, $\boldsymbol{j}$ is the electric current density, p is the fluid pressure, and φ is the electric potential. When the double layer thickness is much smaller than a typical grain surface the transport coefficients are:

$$L_{11} = \frac{k}{\eta} \qquad (3)$$

$$L_{12} = L_{21} = -\frac{\varepsilon\zeta}{\eta F} \qquad (4)$$

$$L_{22} = \sigma_b \qquad (5)$$

Here, k is the fluid-flow permeability, η is the fluid viscosity, ε is the dielectric constant of the fluid, σ_b is the bulk sample conductivity, F is the electrical formation factor (a pore topology term), and ζ is the zeta potential, which is a measure of how much charge resides in the diffuse part of the double layer. The first term

on the right-hand side of Equation (1) is Darcy's Law, the second term of Equation (2) is Ohm's Law, and the remaining terms represent the coupled electrokinetic effect with $L_{12} = L_{21}$ (Onsager, 1931).

Electrokinetic phenomena arise from movement of ions in the electric double layer under a pore pressure gradient. Fluid flow causes mobile ions to be convected relative to the bound charge on the mineral grain surfaces, charge motion known as the convection current. As this charge is deposited at the exit face of the sample and the bound charge is left exposed at the opposite face, a charge separation exists which drives an Ohmic return current, or the conduction current. In the absence of external current sources ($\boldsymbol{j} = 0$), the convection current ($L_{12}\nabla p$) and conduction current ($L_{22}\nabla\varphi$) are equal and opposite and equating them reveals the result of Smoluchowski (1903):

$$Cc = \frac{\Delta\varphi}{\Delta p} = -\frac{L_{12}}{L_{22}} = \frac{\varepsilon\zeta}{\eta F \sigma_b} \qquad (6)$$

where Cc is known as the *streaming potential coupling coefficient* and is classically measured in mV/atm (or mV/0.1MPa). It is via this equation that the zeta potential is often measured in single fluid systems. Although the first expressions in Equation (6) are valid in multi-phase fluid systems (such as the CO_2 / H_2O system studied here), the final expression is not. No theory for the transport coefficients in multi-phase fluid systems is available, and accordingly we did not measure the zeta potential in our CO_2 / H_2O system.

3. Experimental

The testing device contained a cylindrical core of rock 125 mm in length and 25 mm in diameter. Each sample was surrounded by a 3 mm thick Teflon sleeve and inserted into an aluminum cell. PEEK plastic end caps were beveled and flared out the end portions of the Teflon sleeve, insulating the specimen from contact with the aluminum shell. The sample was coated with silicone adhesive before being inserted into the Teflon sleeve to prevent flow at this interface. Prior to testing, the samples were saturated under vacuum with 125 Ω-m tap water.

Each end cap contained 2 electrodes, one copper screw and one steel screw, which were tightened against the sample. Electric potentials across the specimen were recorded at 200 samples / sec. Pressure transducers at each end of the testing device measured absolute fluid pressures every 0.5 sec. Electrode drift was minimal, and electrode polarization was not encountered.

Fluid pressure drop across the sample was regulated using a needle valve at the outlet of the testing device. Inlet CO_2 pressure was maintained at 6.5 MPa. CO_2 was flowed into the samples intermittently throughout a testing period of about one hour, with efforts made to maintain the same CO_2 flow rate between individual tests. CO_2 was injected for 50% of total testing time in a manner such that periods of CO_2 flow were separated by equal intervals of no flow. Following each CO_2 flood, the samples were again saturated with tap water under vacuum.

The five test samples (Berea 1-5) were cored from the same block of Berea sandstone. Testing on samples Berea-1, Berea-2, and Berea-3 determined the streaming potential coupling coefficient (Cc) prior to, during, and after each CO_2 flood. Testing on samples Berea-4 and Berea-5 investigated the resistivity evolution during CO_2 infiltration. In the resistivity tests, an alternating current was applied at 1000Hz with a constant driving voltage of 7V. Resistivity was monitored using two digital multi-meters and recorded every 30 seconds.

4. Results

Testing for the Cc before and after each CO_2 flood was accomplished using a static head at low pressure drops. Results indicated linear correlation between applied pressure drop and observed electric potential. Table 1 summarizes these results, revealing that for specimens Berea-1 and Berea-5 the Cc decreased following the CO_2 flood, while for specimens Berea-2, Berea-3 and Berea-4 the Cc increased. For all five Berea specimens, the gross average Cc for 125 Ω-m water flow was approximately –30 mV / 0.1MPa. Variance shown in Table 1 arises from multiple tests performed on each specimen.

During liquid CO_2 invasion, the Cc evolved in response to the mixing and displacement of pore water. Figure 1 shows the Cc evolution for samples Berea-1, Berea-2 and Berea-3 during the initial 20 minutes of CO_2 infiltration, with

time as a proxy for the volume of CO_2 flowed through the sample. Table 1 lists Cc values for liquid CO_2 flow after the Cc became steady and mixing was assumed to be complete ($t > 700$ sec). The steady-state Cc for liquid CO_2 flow through initially water-saturated samples was approximately −3 mV / 0.1MPa.

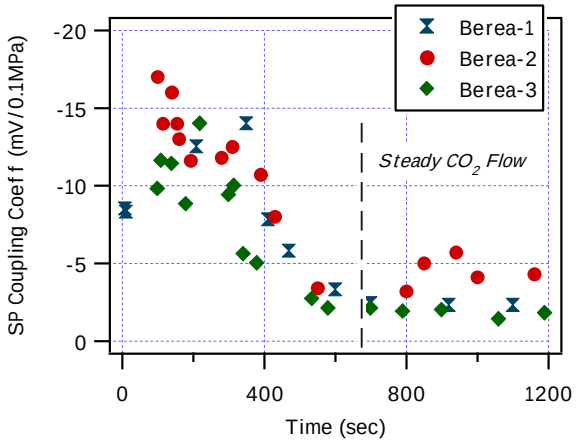

Figure 1. Coupling coefficient vs. time for samples Berea-1, Berea-2 and Berea-3. Only the initial portion of the tests are shown. The Cc was constant for times greater than 700 seconds. The size of the individual symbols approximates experimental variance.

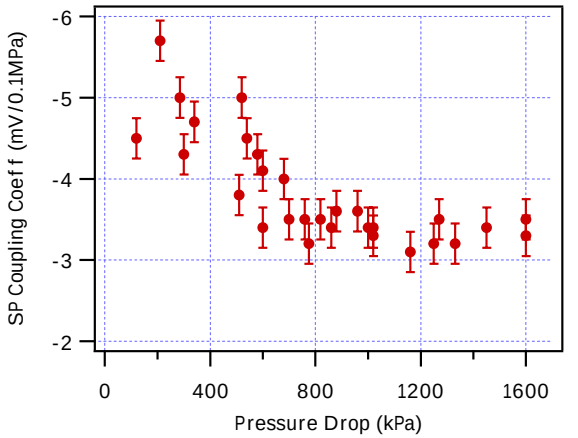

Figure 2. Relationship of Cc to pressure drop for sample Berea-2 from that time after water / CO_2 mixing was assumed to be complete, or $t > 700$ sec (Figure 1). Error bars reflect experimental variation due to pressure and voltage signal noise.

The relationship between coupling coefficient and pressure drop is illustrated in Figure 2. We noted a decrease in the Cc with pressure drop and observed that the Cc tends toward a constant value as pressure drop increases.

We next measured the Cc for liquid CO_2 flow through a dry specimen. This sample was not oven-dried, but rather air-dried for 30 days, and can therefore be assumed to contain only bound water remaining on mineral grain surfaces. We determined the Cc to be −0.02 mV / 0.1MPa for liquid CO_2 flow.

Specimen porosity was measured following each CO_2 flood. For comparison we also measured the porosity of 2 *fresh* cores taken from the same block to be 18.75%. Table 1 lists the porosity of each sample after CO_2 infiltration. Results indicate no change in porosity.

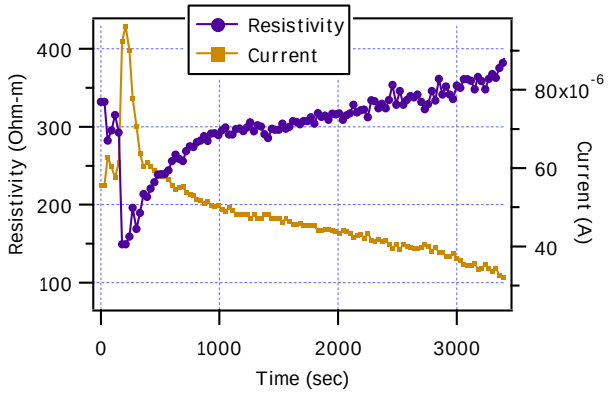

Figure 3. Bulk resistivity and applied current for specimen Berea-5 indicating decreased resistivity during mixing, and only slight change after liquid CO_2 had replaced all mobile water as the pore fluid.

Bulk resistivity variation during liquid CO_2 infiltration was investigated for specimens Berea-4 and Berea-5. Results for specimen Berea-5 are presented in Figure 3, where time is again used as a proxy to represent the volume of CO_2 flowed through the specimen. We observed an initial resistivity of 330 Ω-m, followed by a rapid decrease to 150 Ω-m while the CO_2 and water were mixing. For longer times, when many pore volumes of CO_2 had flowed through the sample, resistivity reached 380 Ω-m.

5. Discussion

The average coupling coefficient for 125 Ω-m tap water flow was −27 mV / 0.1MPa (Table 2), a result within the range of reported values for similar pore fluids (Pengra et al.,

1999; Revil, 2002b). Transport coefficients (L_{12}, L_{22}) for Equations (1) and (2) are reported in Table 2.

Table 1. Summary of coupling coefficient and porosity results. Cc units are mV / 0.1MPa. The average porosity for *fresh* specimens was 18.75%.

Sample	Pre-Flood Cc (water)	Steady-State Cc (CO_2)	Post-Flood Cc (water)	Post-Flood Porosity %
Berea-1	-47 ± 2	-2.5 ± 0.5	-16 ± 1	18.70
Berea-2	-19 ± 0.5	-3.5 ± 0.5	-30 ± 2	18.75
Berea-3	-35 ± 0.5	-2.0 ± 0.5	-41 ± 0.5	18.76
Berea-4	-15 ± 0.5		-18 ± 0.5	18.99
Berea-5	-29 ± 0.5		-21 ± 1	18.64

Table 2. Transport coefficients for Equations (1) and (2). Average Cc is reported with ±1 standard deviation.

Pore Fluid	Average Cc [$-L_{12} / L_{22}$] (mV / 0.1MPa)	L_{22} (S / m)	L_{12} (A / m / Pa)
Water	-27 ± 11	3.0×10^{-3}	0.81×10^{-9}
Liquid CO_2	-2.7 ± 0.7	2.7×10^{-3}	0.073×10^{-9}

According to Archie's Law ($F = \phi^{-m}$), with the exponent $m = 1.9$ (Pengra et al., 1999), and the porosity measured ($\phi = 0.188$), the formation factor (F) was found to be 24. The electrical conductivity of the water-saturated sample was 3.0×10^{-3} S/m (Figure 3). The zeta potential for our rock / water system was thus determined from Equation (6) to be –28 mV, a result within the range of observed values for pore fluids with bivalent cations (Alkafeef et al., 1999). Ca^{++} ion concentrations up to 8 mg/l in our tap water have the effect of decreasing the zeta potential by a factor of two compared to monovalent cation solutions (Lorne et al., 1999).

The observation of *any* streaming potential in the presence of non-conducting liquid CO_2 indicates lasting effects of trapped and bound water. As the pore water was initially displaced by invading CO_2, the Cc decreased (Figure 1). At longer times all mobile pore water was displaced, but *trapped water* remained, and the Cc became steady at about −3 mV / 0.1MPa. Flowing CO_2 may be shearing the trapped water resulting in counter charge displacement from water layers. Trapped water then acts as a pathway for return electrical conduction. The combined effect explains the apparent steady-state *trapped water* limit of the streaming potential.

To test the hypothesis that trapped water is controlling the electrokinetic response, we measured the Cc for liquid CO_2 flow through an air-dried specimen that was assumed to have only bound water remaining on the mineral surfaces. The results reveal a *bound water* limit of the Cc to be −0.02 mV / 0.1MPa which is 2 orders of magnitude lower than the Cc for an initially water-saturated sample. This indicates that significant water remained in the initially saturated specimens even after a steady Cc was attained.

The relatively minor change in bulk resistivity as liquid CO_2 infiltrated the specimens supports the hypothesis that trapped water is controlling electrical conduction. For longer times, and therefore greater pore volumes of CO_2, all mobile pore water had been displaced, yet the sample resistivity was only slightly higher (380 Ω-m) than when it was originally water saturated (330 Ω-m). These results are in spite of the fact that liquid CO_2 may be up to one million times more resistive than water.

Employing a linear model for electrical conductivity (Lorne et al., 1999; Revil, 2002a):

$$\sigma_b \cong \frac{\sigma_f}{F} + \sigma_s \qquad (7)$$

where σ_f is the conductivity of the pore fluid (8.0×10^{-3} S/m), we calculate the surface conductivity to be $\sigma_s = 2.7 \times 10^{-3}$ S/m. When insulating liquid CO_2 has replaced all mobile water as the pore fluid, the bulk sample conductivity is equal to only the surface conductivity ($\sigma_b \approx \sigma_s$), or the resistivity ($\rho_b = 1/\sigma_s$) is 375 Ω-m, consistent with the limiting value shown in Figure 3.

The pH of the pore fluid strongly effects the zeta potential and consequently the Cc (Ishido and Mizutani, 1981; Revil et al., 1999). During CO_2 infiltration, the pH will decrease with the formation of weak carbonic acid resulting in a decrease in the zeta potential and Cc. The resistivity decrease observed during mixing may similarly reflect a pH change as the formation of

acid adds ions available for electrical conduction. Fully characterizing the effect of pH on the zeta potential and Cc requires in situ measurement of the pH of the pressurized pore fluid which is currently unfeasible.

For liquid CO_2 flow, pressure drops across the samples were typically quite high due to the high internal pressure of the testing device and limitations of the pressure control system. Variability of the Cc with pressure drop has been reported, with the Cc being constant for low pressure drops, and decreasing for greater pressure drops (Morgan, et al., 1989). Most commonly, the Cc is measured for small pressure gradients similar to those encountered in groundwater systems. Our results, however, are more applicable to zones near CO_2 injection points where pressure gradients may be quite high. For areas farther away from the injection point, the Cc will be greater as indicated in part by the data shown in Figure 2.

Changes in the Cc determined before and after each CO_2 flood were initially thought to be caused by changes in sample porosity. Carbonic acid formed by mixing CO_2 and water may have dissolved the mineral ankerite which is present in minor fractions (~0.5%) in Berea sandstone. The resulting change in the pore fabric could result in higher functional porosity and explain the increase in Cc observed following the CO_2 flood (Revil et al., 1999). However, we were unable to detect any change in porosity.

Another possible explanation for the observed change in the Cc following each CO_2 flood is permeability changes caused by release and capture of matrix particles, especially kaolinite clays. The concept of particle release and capture by both chemical and mechanical means is discussed by Ochi and Vernoux (1998). In our testing, variable flow conditions between specimens may have resulted in permeability changes following each CO_2 flood that would cause corresponding changes in the Cc. Correlation between the Cc and permeability has been demonstrated for samples undergoing deformation, but the intrinsic dependence is as yet unclear (Jouniaux and Pozzi, 1995; Lorne et al., 1999).

Pressure of about 5.7 MPa is required to maintain CO_2 at single-phase liquid conditions at 20°C. In our tests, the inlet pressure was held constant at 6.5 MPa, but the maximum tested pressure drop across the samples was 1.6 MPa. Therefore, the fluid may have entered the two-phase liquid / gas regime. Recent works that have quantified the Cc in 2-phase conditions have noted that the Cc decreases with increasing gas content, despite the increase in resistivity (Guichet, et al., 2003; Revil and Cerepi, 2004). We observed a nearly constant Cc following CO_2 / water mixing, and although we may have inadvertently had some CO_2 gas present for some of the larger pressure drops, we feel the effect was minimal.

6. Conclusion

This testing revealed an average Cc of about −30 mV / 0.1MPa for water flow through a *water-saturated* sample of Berea sandstone. Liquid CO_2 then invaded and displaced mobile pore water until only *trapped water* remained, and the Cc was found to be −3 mV / 0.1MPa. For liquid CO_2 flow in an air-dried sample where only *bound water* initially existed, the Cc was −0.02 mV / 0.1MPa. Bulk resistivity variation during CO_2 infiltration was marked by a decline during mixing where the formation of acid aided electrical conduction. Results suggest that trapped and bound water in the sample control the electrokinetic response.

Acknowledgements

This work was supported in part by the U.S. Dept. of Energy contract DE-AC07-991D13727 to the Idaho Natl. Eng. and Env. Laboratory. The authors thank André Revil and Steven Pride for insightful reviews and input. This work benefited greatly from their generous contributions. We also thank the UC Center for Information Technology Research in the Interest of Society, and the NSF CMS division for additional facilities and funding.

References

Alkafeef, S. F., R. J. Gochin, and A. L. Smith (1999), Measurement of the electrokinetic potential at reservoir rock surfaces avoiding the effect of surface conductivity, *Colloid Surface A*, *159,* 263-270.

Corwin, R. F., and D. B. Hoover, (1979), The self potential method in geothermal exploration; *Geophysics, 44*(2), 226-245.

Fagerlund, F., and G. Heinson (2002), Detecting subsurface groundwater flow in fractured rock using self-potential (SP) methods, *Environ. Geol., 43*, 782-794.

Guichet, X., L. Jouniaux, and J. Pozzi (2003), Streaming potential of a sand column in partial saturation conditions, *J. Geophys. Res., 108*(B3), 2141, doi:10.1029/2001JB001517.

Ishido, T., and H. Mizutani (1981), Experimental and theoretical basis of electrokinetic phenomena in rock-water systems and its applications to geophysics, *J. Geophys. Res., 86*(B3), 1763-1775.

Jouniaux, L., and J. Pozzi (1995), Streaming potential and permeability of saturated sandstones under triaxial stress: consequences for electrotelluric anomalies prior to earthquakes, *J. Geophys. Res., 100*(B6), 10,197-10,209.

Lorne, B., F. Perrier, and J. Avouac (1999), Streaming potential measurements 1. Properties of the electric double layer, *J. Geophys. Res., 104*(B8), 17,857-17,877.

Morgan, F., E. Williams, and T. Madden (1989), Streaming potential properties of westerly granite with applications, *J. Geophys. Res., 94(*B9*)*, 12,449-12,461.

Ochi, J., and J. F. Vernoux (1998), Permeability decrease in sandstone reservoirs by fluid injection: Hydrodynamic and chemical effects, *J. Hydrol., 208*, 237-248.

Onsager, L., (1931) Reciprocal relations in irreversible processes, 1, *Phys. Rev. 37*, 405-426.

Pengra, D. B., S. X. Li, and P. Wong (1999), Determination of rock properties by low-frequency AC electrokinetics, *J. Geophys. Res., 104*(B12), 29,485-29,508.

Pride, S. (1994), Governing equations for the coupled electromagnetics and acoustics of porous media, *Phys. Rev. B*, *50*(21), 15,678-15,696.

Revil, A., H. Schwaeger, L. M. Cathles, and P. Manhardt (1999), Streaming potential in porous media 2. Theory and applications to geothermal systems, *J. Geophys. Res., 104*(B9) 20,033-20,048.

Revil, A. (2002a), The hydroelectric problem of porous rocks: thermodynamic approach and introduction of a percolation threshold, *Geophys. J. Int., 151*(3), 944-949.

Revil, A. (2002b), Comment on "Rapid Fluid Disruption: A source for self-potential anomalies on volcanoes" by M. J. S. Johnston, J. D. Byerlee, and D. Lockner, *J. Geophys. Res., 107*(B8), 2155, doi:10.1029/2001JB000788.

Revil, A., and A. Cerepi (2004), Streaming potentials in two-phase conditions, *Geophys. Res. Lett., 31*, L11605, doi:10.1029/2004GL020140.

Sill, W. R. (1983), Self-potential modeling from primary flows, *Geophysics, 48*(1), 76-86.

von Smoluchowski, M. (1903), Contribution à la théorie de l'endosmose électrique et de quelques phenomènes corrélatifs, *Bulletin International de l'Academie des Sciences de Cracovie, 8,* 182-200.